



Published in final edited form as:

*Appl Magn Reson*. 2008 ; 34(3-4): 533–544. doi:10.1007/s00723-008-0136-2.

## DNP-Hyperpolarized $^{13}\text{C}$ Magnetic Resonance Metabolic Imaging for Cancer Applications

S. J. Nelson<sup>1</sup>, D. Vigneron<sup>1</sup>, J. Kurhanewicz<sup>1</sup>, A. Chen<sup>1</sup>, R. Bok<sup>1</sup>, and R. Hurd<sup>2</sup>

<sup>1</sup> University of California San Francisco, San Francisco, California, USA

<sup>2</sup> GE Healthcare, Menlo Park, California, USA

### Abstract

Critical factors in characterizing the aggressiveness and response to therapy for tumors are the availability of noninvasive biomarkers that can be combined with other clinical parameters to tailor treatment regimens to each individual patient. While conventional magnetic resonance (MR) images are widely used to estimate changes in tumor size, they do not provide the rapid readout that is required to make an early decision on whether a change in therapy is required. The use of hyperpolarized  $^{13}\text{C}$  agents to obtain metabolic imaging data is of great interest for in vivo assessment of tumors. One of the first agents being considered for in vivo studies with dynamic nuclear polarization (DNP) is 1- $^{13}\text{C}$ -labeled pyruvate, which is converted to lactate or alanine, dependent upon the needs of the tissue in question. The development of this new technology and its implementation in preclinical cancer model systems has clearly demonstrated the potential for highlighting tumor aggressiveness and for monitoring changes associated with disease progression. While there is further work to do in terms of studying new agents, improving the DNP process itself and developing efficient MR methods for acquiring and analyzing the data, the preliminary results are extremely promising and provide strong motivation for considering cancer as one of the first applications of the technology.

### 1 Introduction

The development of technology that applies dynamic nuclear polarization (DNP) to generate hyperpolarized  $^{13}\text{C}$  agents and a dissolution process that prepares them for injection into living subjects means that it is now possible to investigate in vivo applications. The prototype polarizer that was designed in Malmo, Sweden [1–5] has been shown to provide a higher than 10000-fold signal enhancement for detecting  $^{13}\text{C}$  probes of endogenous, nontoxic, nonradioactive substances such as pyruvate and to have the potential for monitoring fluxes through multiple key biochemical pathways such as glycolysis [6,7], the citric acid cycle [8, 9] and fatty acid synthesis [10,11]. Preliminary studies that were performed in a whole-body magnetic resonance (MR) scanner at 1.5 T in rat kidney [12] and in tumors [4,13,14] have confirmed that 1- $^{13}\text{C}$ -labeled pyruvate is delivered to tissues and converted to alanine, lactate and bicarbonate with a spatial distribution and time course that varies according to the tissue of interest.

There is already considerable evidence that in vivo metabolic imaging is important for the characterization and evaluation of response to therapy for prostate and brain cancers [15,16]. Patient studies using  $^1\text{H}$  MR spectroscopic imaging have demonstrated that there are distinct

metabolic signatures between the normal tissue and the tumor that can be used to define the spatial extent of the lesion and to distinguish between high- and low-grade tumors [15–20]. The presence of elevated choline is an ubiquitous finding for tumors and is accompanied by a decrease in levels of normal metabolites. In the brain, high-grade tumors are distinguished by the presence of lactate and lipid, with high levels of each of these being predictive of poor outcome for patients with newly diagnosed lesions [17]. For the prostate, the data acquisition sequence used for in vivo  $^1\text{H}$  spectroscopic imaging applies a frequency-selective pulse in order to eliminate the contribution from peri-prostatic lipid and this precludes the measurement of lactate [21,22]. It has therefore not been possible to establish a direct relationship between levels of lactate and outcome for these patients. In this case, the evidence for lactate being a marker of aggressiveness for prostate cancer has therefore come from ex vivo measurements of human biopsy samples [23].

Further investigation of the application of hyperpolarized  $^{13}\text{C}$  metabolic imaging in order to evaluate lactate and other compounds requires the development of rapid data acquisition and analysis techniques, followed by the evaluation of appropriate agents and measurements of their action in animal models that represent both normal tissue and cancer. In the following, we describe initial studies in rodents and dogs that were obtained following an injection of hyperpolarized  $^{13}\text{C}$ -pyruvate using a 3 T whole-body scanner. DNP systems used for these studies were a prototype system that was constructed in Malmo and one of the first commercial HyperSense systems made by Oxford Instruments under license to GE Healthcare. The methodologies being applied are first reviewed and then the preliminary studies being performed in preparation for applications in humans are discussed.

## 2 The DNP Technique

The methodology used for in vivo studies is based on polarizing nuclear spins in an amorphous solid state at about 1 K through coupling of the nuclear spins with unpaired electrons that are added to the sample via an organic free radical. In the amorphous solid state, high electron spin polarization is in part transferred to the nuclear spins using microwave irradiation. Critical to the in vivo use of this method is the ability to bring the polarized, cold sample into solution while preserving its nuclear polarization as described in refs. 1–5. The initial publications demonstrated that the prototype system developed in Malmo could achieve polarizations of as high as 37% for  $^{13}\text{C}$  and 7.8% for N-15 can be obtained after dissolution of the polarized solid, with corresponding signal enhancements of 44400- and 23500-fold, respectively [1]. The HyperSense polarizer has an underlying design similar to the original but has a more automated dissolution procedure. It also operates at a temperature of 1.4 K compared with 1.2 K for the prototype system, which means that the maximum level of polarization it can achieve is lower. After dissolution, the hyperpolarized liquid sample is collected in a sample cup, drawn up into a syringe and taken as rapidly as possible into the scan room for injection into the subject. Once injected the sample may be used as a probe for many different types of in vivo imaging or spectroscopy. One of the first examples was the acquisition of  $^{13}\text{C}$  angiography data with a signal-to-noise ratio (S/N) of approximately 275 that was acquired within approximately 0.25 s after the injection of hyperpolarized aqueous  $^{13}\text{C}$ -urea solution in rat [24]. Other animal studies with hyperpolarized  $^{13}\text{C}$  have utilized fast imaging sequences with limited spectral information [14,25–27]. The studies described here have applied fast  $^{13}\text{C}$  spectroscopic imaging techniques with greater efficiency, cover age, speed and spectral resolution to provide an improved monitoring of metabolic pathways.

## 3 Selection of a Hyperpolarized Agent

The choice of a hyperpolarized substrate is based both on metabolic and MR properties. A long  $T_1$  is required to maintain the polarization until the time of in vivo imaging.  $T_1$ s of  $^{13}\text{C}$  in small

molecules are significantly longer ( $> 10$  s), particularly when the  $^{13}\text{C}$  is a carbonyl carbon with no nearby protons. The C-1 carbonyl of pyruvate has  $T_1$  of approximately 45 s in blood. A further advantage of using  $^{13}\text{C}$  is that unlabeled tissues are virtually invisible so that signals from the hyperpolarized substrate and subsequent metabolic products provide the dominant contribution to the corresponding data. These considerations have led to pyruvate being used as one of the first hyperpolarized substrates in animal studies [4,12]. In particular, pyruvate that was labeled at the C-1 position has been injected into rats and pigs so that both the original  $^{13}\text{C}$ -pyruvate and its metabolic products  $^{13}\text{C}$ -alanine and  $^{13}\text{C}$ -lactate could be observed. This technique has allowed for the acquisition of  $^{13}\text{C}$  MR spectroscopy (MRS) data with very high temporal resolution (in the order of seconds) and the observation of real-time, tissue-specific metabolic changes. New agents with improved capabilities for crossing the blood–brain barrier and for monitoring different metabolic pathways are also being considered.

#### 4 Radio Frequency Coils for Hyperpolarized $^{13}\text{C}$ Studies

Since the metabolism detected by hyperpolarized  $^{13}\text{C}$  agents occurs in vivo, animal studies are required for technique testing and evaluation. The first study conducted was to verify that the DNP equipment and methodology developed to acquire data using a 3 T whole-body scanner would give results similar to the data obtained by Golman et al. [4]. To perform these experiments it was necessary to design new pulse sequences and to develop appropriate radio frequency (rf) coils for use at 3 T. The specialized coil that was constructed had a linear  $^1\text{H}$  component and a quadrature  $^{13}\text{C}$  component [28]. As is shown below, these initial studies showed an excellent S/N ratio as measured by the heights of the metabolite peaks in the spectra divided by the root-mean-square of the signal in the regions of the spectrum that were devoid of metabolites. Other rf coils that were designed and constructed included a quadrature  $^1\text{H}$ –quadrature  $^{13}\text{C}$  mouse coil and an associated holder [29], a volume  $^{13}\text{C}$  transmit and a dual  $^1\text{H}$ – $^{13}\text{C}$  receive endorectal coil that were designed for humans but could also be used for dog studies [30,31].

#### 5 In Vivo Hyperpolarized $^{13}\text{C}$ from Rats at 3 T

Hyperpolarized  $^{13}\text{C}$  pyruvate was obtained using DNP as described previously and 3.5 ml of hyperpolarized solution was injected into the tail vein of anesthetized normal Sprague-Dawley rats within 30 s of dissolution. The rats were imaged in the homebuilt dual-tuned rat coil using the 3 T clinical scanner. Dynamic nonlocalized  $^{13}\text{C}$  MR spectra (Fig. 1b) were acquired from 4 rats with a 3 s time resolution and  $10^\circ$  tip angle. Calibration of the RF power for determining the tip angle was achieved at the  $^{13}\text{C}$  frequency. These data demonstrated the uptake and the time course of the hyperpolarized  $^{13}\text{C}$ -pyruvate and its metabolic products  $^{13}\text{C}$ -lactate,  $^{13}\text{C}$ -alanine and  $^{13}\text{C}$ -bicarbonate. Two-dimensional (2-D)  $^{13}\text{C}$  MRS images (Fig. 1c) were acquired from eight rats starting 15 s after injection following the original protocol developed by researchers from GE Healthcare. A 4 cm axial slice centered at the level of kidneys was collected with a field of view (FOV) of 80 by 80 mm, a time repetition (RT) of 80 ms, a spectral width of 5000 Hz and 256 spectral points. Metabolite images in Fig. 1c are presented as magnitude color overlays on a grayscale proton reference image and show different metabolic distributions for different organs. Although these initial studies [28] had relatively low levels of polarization that ranged from 1.8% to 14.1%, they clearly demonstrated the feasibility of using hyperpolarized  $^{13}\text{C}$ -pyruvate for an in vivo experiment on a commercial 3 T MR scanner to observe its conversion into lactate, alanine, and bicarbonate.

## 6 Hyperpolarized $^{13}\text{C}$ MRS Imaging in a Murine Model of Prostate Cancer at 3

### T

The first dynamic-hyperpolarized  $^{13}\text{C}$  MRS imaging studies of prostate tumors were performed at various stages of progression using the transgenic adenocarcinoma of mouse prostate (TRAMP) mouse that was engineered by Greenberg et al. [32,33]. The TRAMP model is particularly useful for following changes that occur with prostate cancer evolution, since the metabolic and histopathologic features that are associated with the disease progression mimic those of the human disease [33]. Early-stage tumors are relatively small and contain a significant number of well differentiated epithelium. As the tumors progress, the glandular architecture of the prostate is replaced by poorly differentiated epithelium and there may be metastatic spread to the lymph nodes. Large, late-stage tumors are more heterogeneous and may include regions of necrosis. The goal of the initial  $^{13}\text{C}$  studies was to assess the feasibility of detecting hyperpolarized pyruvate and its metabolic products within such model systems. In order to obtain 3-D metabolic images throughout the animal, a new echo planar spectroscopic imaging (EPSI) technique was developed to detect  $^{13}\text{C}$ -pyruvate and its metabolic products in primary and metastatic tumors as well as normal tissues [29,35]. This double spin-echo sequence uses low tip angles to retain the polarization as long as possible and echo planar sampling in one spatial dimension to reduce the number of excitations required. The sequence also includes the possibility of selecting an option that applies excitations with variable tip angles in order to use the magnetization more effectively.  $T_2$ -weighted high-resolution  $^1\text{H}$  MR images in sagittal, axial and coronal views were acquired to correlate with the anatomy as shown in Fig. 2.

Dynamic-hyperpolarized  $^{13}\text{C}$  spectroscopic imaging was performed 35 s after the injection of a solution of hyperpolarized  $^{13}\text{C}$  pyruvate into the tail vein of the anesthetized mouse. The compound polarized was a mixture of pyruvic acid- $1\text{-}^{13}\text{C}$  and the trityl radical (tris {8-carboxyl-2,2,6,6-tetra[2-(1-hydroxyethyl)]-benzo(1,2-d:4,5-d')bis(1,3)dithiole-4-yl} methyl sodium salt) obtained from GE Healthcare. The mixture contained 91% pyruvic acid. TRIS-EDTA dissolution medium was used to bring the final dissolved sample to the desired concentration and pH level. Two different concentrations, 79 and 250 mM, of the hyperpolarized pyruvate solution were used. An aliquot of the pyruvate solution was used to measure the percent polarization, as well as the pH of the final solution. In each of the mice studied, 0.35 ml of the final pyruvate solution was injected into the mouse over a 12 s period followed by 0.2 ml of normal saline flush.

The  $^{13}\text{C}$  metabolic imaging data were acquired using a double spin-echo pulse sequence that provided 3-D localization at a nominal spatial resolution of  $0.135\text{ cm}^3$  in 10 s. Data analysis was performed offline using a custom software developed in our research group. As shown in Figs. 2–5, these preliminary studies clearly demonstrated the feasibility of obtaining high-resolution  $^{13}\text{C}$  MRS imaging data with high S/N ratio from normal and TRAMP mice by injecting a hyperpolarized  $^{13}\text{C}$  substrate in animals. The first set of studies used the prototype polarizer for one normal and four TRAMP mice. Polarization levels obtained varied from 17% to 21% [29]. Similar results were subsequently obtained using the HyperSense polarizer with levels of polarization ranging from 15% to 20% (Figs. 3 and 4). Different  $^{13}\text{C}$  metabolic characteristics were observed in mouse kidney, liver, normal prostate and prostate tumor (Fig. 3) and heterogeneity was seen within large tumors (Fig. 4). These preliminary studies also demonstrated (Fig. 5) that an increase in lactate-to-pyruvate ratio could be observed during the progression from early- to later-stage tumors.

While  $^1\text{H}$  spectroscopy provides valuable metabolic information on prostate cancer, the high sensitivity of hyperpolarized  $^{13}\text{C}$  MRS and its ability to monitor  $1\text{-}^{13}\text{C}$ -labeled pyruvate and its metabolic products (lactate and alanine) has the potential to improve the characterization

of prostate cancer. Fast  $^{13}\text{C}$  3-D MRS imaging data from the TRAMP mouse clearly demonstrated that high levels of lactate were produced from hyperpolarized  $^{13}\text{C}$  pyruvate in both primary and metastatic tumors, and that there was an increase in lactate production with disease progression (Fig. 5). A more recent study that acquired data from four normal mice, four TRAMP mice with early-stage tumors and three TRAMP mice with late-stage tumors has demonstrated a pathologic-grade-dependent increase in lactate and to a lesser degree in alanine [34]. These studies have demonstrated the feasibility of providing noninvasive biomarkers for characterizing the tumor aggressiveness and the potential for serially monitoring disease progression and potentially response to therapy using hyperpolarized  $^{13}\text{C}$  metabolite imaging.

## 7 Hyperpolarized $^{13}\text{C}$ MRS Imaging Data of Dog Prostate at 3 T

As described above, hyperpolarized  $^{13}\text{C}$ -pyruvate has been used to image metabolism in preclinical experiments within rodents and other small animals. The objective of the initial study in dogs was to perform experiments that would evaluate the feasibility of observing changes in hyperpolarized  $^{13}\text{C}$ -pyruvate and its products by in vivo MRS imaging techniques at a larger scale. The choice of a dog model was dictated by the fact that the anatomy of its prostate is similar to that of the human. This meant that the coil geometry and data acquisition parameters used would provide a realistic test of the methodology. Specific goals of the study were to test the rf coils (Fig. 6) and pulse sequences, being developed, to determine the dynamics of arrival of the pyruvate bolus, to evaluate the use of pyruvate in healthy dog prostate and to see whether its metabolic products could be observed with a 3 T MR scanner.

In the initial studies, six dogs were sedated and maintained under anesthesia at 37 °C with a heating blanket. A volume  $^{13}\text{C}$  transmit coil and endorectal  $^{13}\text{C}$ - $^1\text{H}$  receive coil were positioned, and the animal was advanced into the bore of the 3 T scanner. Polarizations were performed using the system developed at GE Healthcare and installed in a room adjacent to the 3 T MR scanner (Fig. 6a). Two to three injections were performed in each animal, separated by approximately 90 min. The levels of polarization were very reproducible with a mean of 19.7% and a standard deviation of 1.4%. The amount of  $^{13}\text{C}$ -labeled pyruvate for each dog was calculated on the basis of delivery of 250 mM at a dose volume of 1.4 ml/kg of body weight. A 10 ml saline flush was used to ensure that the infusion line was emptied of the pyruvate solution. The injections were done automatically using an Ulrich Mississippi power injector. The MR protocol comprised four components: conventional FSE imaging to define the anatomy, nonlocalized dynamic  $^{13}\text{C}$  spectroscopy, 2-D  $^{13}\text{C}$  MRS imaging with conventional phase encoding (FastCSI) and 3-D  $^{13}\text{C}$  EPSI. Figure 6 shows an example of the data acquired. The reconstruction and analyses of the  $^{13}\text{C}$  MR data were performed using the SAGE package from GE Healthcare and an in-house software package. Although some features needed to be adapted to accommodate the rapid acquisition and specialized features of the  $^{13}\text{C}$  experiments, the basic architecture and display features of these packages were similar to those developed for  $^1\text{H}$  spectroscopic imaging. The lactate peak occurred, on average, 15 s later than the pyruvate peak. The average arrival time for the pyruvate was 26 s (range of 24–30 s) and the pyruvate peak was 43 s (range of 39–48 s). There were relatively low levels of alanine and bicarbonate in all dogs studied. The S/N ratio for the chemical shift imaging data varied from 154:1 to 361:1 for pyruvate and 25:1 to 67:1 for lactate. As expected, the use of a fly-back echo planar trajectory for the 3-D EPSI acquisition provided a 50% loss in S/N ratio, but the spectral quality was still excellent and provided volumetric coverage.

These studies provided strong evidence for the feasibility of translating the hyperpolarized  $^{13}\text{C}$  technology for evaluating in vivo metabolic processes in the prostate to larger animal models and eventually patients. The hyperpolarized  $^{13}\text{C}$  metabolic imaging data showed that pyruvate is taken up rapidly in the dog prostate and partially is converted into lactate. The observed lactate-to-pyruvate ratios were significantly lower than previously seen

in studies of the rat kidney and in mouse tumors but were still detected by the 3-D EPSI sequence with an isotropic spatial resolution of  $0.125 \text{ cm}^3$ . Levels of alanine in the dog prostate were relatively low, which is consistent with previous measurements in human biopsies from a normal, healthy prostate tissue. Further improvements in the MR data acquisition techniques [35–38], in conjunction with more sophisticated postprocessing algorithms, are likely to provide data with improved coverage and/or finer spatial resolution.

## 8 Future Directions

There are substantial technical challenges to developing this methodology and translating it into a clinical tool for evaluation of cancer or other diseases. The start point is the availability of appropriate  $^{13}\text{C}$  tracers and the polarizer equipment that can generate the hyperpolarized sample so that it can be delivered to the subject with a delay time of the order of 15–20 s. The  $^{13}\text{C}$  tracer being evaluated in these initial studies is pyruvate, but many other options could be considered. For these initial studies the trityl radical was not removed from the sample preparation before injection into subjects. Although there were no adverse events of either the pyruvate and trityl in any of the animals studied, the range of pyruvate doses that are safe for human studies needs to be evaluated and it is likely that the trityl would be removed from the solution for these purposes. Nowadays there is only a small number of polarizers that use the DNP and dissolution process described above for in vivo applications. The prototype system at University of California San Francisco is sited in a clean room environment adjacent to a 3 T whole-body MR scanner, where it can be used to develop new techniques and obtain research data from humans and animal models. Similar results have been obtained in animal model systems using both this prototype system and the commercial HyperSense system from Oxford Instruments. The initial focus has been on prostate cancer, where it is expected that this new metabolic imaging technique will have a major clinical impact. The methods being developed are expected to have general applicability to a wide variety of cancers and other pathologies. Research studies of brain tumors and liver cancer model systems are under way, but the full potential and applicability of this unprecedented new metabolic imaging modality remain to be determined.

## References

1. Ardenkjaer-Larsen JH, Fridlund B, Gram A, Hansson G, Hansson L, Lerche MH, Servin R, Thaning M, Golman K. *Proc Natl Acad Sci USA* 2003;100:10158–10163. [PubMed: 12930897]
2. Golman K, Olsson LE, Axelsson O, Mansson S, Karlsson M, Petersson JS. *Br J Radiol* 2003;76:118–127.
3. Golman K, Petersson JS. *Acad Radiol* 2006;13:932–942. [PubMed: 16843845]
4. Golman K, in't Zandt R, Lerche M, Pehrson R, Ardenkjaer-Larsen JH. *Cancer Res* 2006;66:10855–10860. [PubMed: 17108122]
5. Wolber J, Ellner F, Fridlund B, Gram A, Jóhannesson H, Hansson G, Hansson L, Lerche MH, Mansson S, Servin R, Thaning M, Golman K, Ardenkjaer-Larsen JH. *Nucl Instrum Methods Phys Res A* 2004;526:173–181.
6. Costello LC, Franklin RB. *Mol Cell Biochem* 2005;280:1–8. [PubMed: 16511951]
7. Gillies RJ, Gatenby RA. *J Bioenerg Biomembr* 2007;39:251–257. [PubMed: 17624581]
8. Costello LC, Franklin RB. *Urology* 1997;50:3–12. [PubMed: 9218011]
9. Costello LC, Franklin RB. *Prostate* 1998;35:285–296. [PubMed: 9609552]
10. Kuhajda FP. *Cancer Res* 2006;66:5977–5980. [PubMed: 16778164]
11. Swinnen JV, Brusselmans K, Verhoeven G. *Curr Opin Clin Nutr Metab Care* 2006;9:358–365. [PubMed: 16778563]
12. Kohler SJ, Yen Y, Wolber J, Chen AP, Albers MJ, Bok R, Zhang V, Tropp J, Nelson S, Vigneron DB, Kurhanewicz J, Hurd RE. *Magn Reson Med* 2007;58:65–69. [PubMed: 17659629]

13. Chen AP, Albers MJ, Cunningham CH, Kohler SJ, Yen YF, Tropp J, Bok R, Pauly JM, Nelson SJ, Kurhanewicz J, Vigneron DB. *Magn Reson Med* 2007;58:65–69. [PubMed: 17659629]
14. Golman K, Ardenkjaer-Larsen JH, Petersson JS, Mansson S, Leunbach I. *Proc Natl Acad Sci USA* 2003;100:10435–10439. [PubMed: 12930896]
15. Kurhanewicz J, Swanson MG, Nelson SJ, Vigneron DB. *J Magn Reson Imag* 2002;16:451–463.
16. Nelson SJ. *Mol Cancer Ther* 2003;2:497–507. [PubMed: 12748312]
17. Li X, Jin H, Lu Y, Oh J, Chang S, Nelson SJ. *NMR Biomed* 2004;17:10–20. [PubMed: 15011246]
18. Li X, Vigneron DB, Cha S, Graves EE, Grawfird F, Chang S, Nelson SJ. *Am J Neuroradiol* 2005;26:760–769. [PubMed: 15814918]
19. McKnight TR, Lamborn KR, Love TD, Berger MS, Chang S, Dillon WP, Bollen A, Nelson SJ. *J Neurosurg* 2007;106:660–666. [PubMed: 17432719]
20. Zakian KL, Sircar K, Hricak H, Chen HN, Shukla-Dave A, Eberhardt M, Muruganandham M, Ehora L, Kattan MW, Reuter VE, Scardino PT, Koutcher JA. *Radiology* 2005;234:804–814. [PubMed: 15734935]
21. Schricker AA, Pauly JM, Kurhanewicz J, Swanson MG, Vigneron DB. *Magn Reson Med* 2001;46:1079–1087. [PubMed: 11746572]
22. Tran TK, Vigneron DB, Sailasuta N, Tropp J, Le Roux P, Kurhanewicz J, Nelson SJ, Hurd R. *Magn Reson Med* 2000;43:23–33. [PubMed: 10642728]
23. Tessem, M.; Keshari, K.; Joun, D., et al. Joint Annual Meeting ISMRM-ESMRMB 2007 Proceedings; Berkeley, Calif. International Society for Magnetic Resonance in Medicine; 2007.
24. Golman K, Ardenkjaer-Larsen JH, Petersson JS, Mansson S, Leunbach I. *Proc Natl Acad Sci USA* 2003;100:10435–10439. [PubMed: 12930896]
25. Johansson E, Mansson S, Wirestam R, Svensson J, Petersson JS, Golman K, Stahlberg F. *Magn Reson Med* 2004;51:464–472. [PubMed: 15004786]
26. Mansson S, Johansson E, Magnusson P, Chai CM, Hansson G, Petersson JS, Stahlberg F, Golman K. *Eur Radiol* 2006;16:57–67. [PubMed: 16402256]
27. Svensson J, Mansson S, Johansson E, Petersson JS, Olsson LE. *Magn Reson Med* 2003;50:256–262. [PubMed: 12876701]
28. Kohler SJ, Yen Y, Wolber J, Chen AP, Albers MJ, Bok B, Zhang V, Tropp J, Nelson S, Vigneron DB, Kurhanewicz J, Hurd RE. *Magn Reson Med* 2007;58:65–69. [PubMed: 17659629]
29. Chen A, Albers M, Kohler S, Cunningham CH, Kohler SJ, Xen Y-F, Hurd RE, Tropp J, Bok R, Pauly JM, Nelson SJ, Kurhanewicz J, Vigneron DB. *Magn Reson Med*. 2007 in press.
30. Nelson, S.; Chen, A.; Bok, R., et al. Joint Annual Meeting ISMRM-ESMRMB 2007 Proceedings; Berkeley, Calif. International Society for Magnetic Resonance in Medicine; 2007. p. 536
31. Tropp, J.; Calderon, P.; Carvajal, L.; Karpodinis, K.; Chen, A.; Vigneron, D.; Hurd, R. ISMRM Fourteenth Meeting Proceedings; Berkeley, Calif. International Society for Magnetic Resonance in Medicine; 2007. p. 501
32. Albers, MJ.; Chen, AP.; Bok, R., et al. Joint Annual Meeting ISMRM-ESMRMB 2007 Proceedings; Berkeley, Calif. International Society for Magnetic Resonance in Medicine; 2007.
33. Greenberg NM, DeMayo F, Finegold MJ, Medina D, Tilley W, Aspinall JO, Cunha GR, Donjacour AA, Matusik RJ, Rosen JM. *Proc Natl Acad Sci USA* 1995;92:3439–3443. [PubMed: 7724580]
34. Albers, M.; Zektzer, A.; Kurhanewicz, J. ISMRM Thirteenth Meeting Proceedings; Berkeley, Calif. International Society for Magnetic Resonance in Medicine; 2005.
35. Cunningham CH, Chen AP, Albers MJ, Kurhanewicz J, Hurd RE, Yen YE, Pauly JM, Nelson SJ, Vigneron DB. *J Magn Reson* 2007;187:357–362. [PubMed: 17562376]
36. Levin YS, Mayer D, Yen YF, Hurd RE, Spielman DM. *Magn Reson Med* 2007;58:245–252. [PubMed: 17654596]
37. Mayer D, Kim DH, Adalsteinsson E, Spielman DM. *Magn Reson Med* 2006;55:974–978. [PubMed: 16586451]
38. Mayer D, Levin YS, Hurd RE, Glover GH, Spielman DM. *Magn Reson Med* 2006;56:932–937. [PubMed: 16941617]

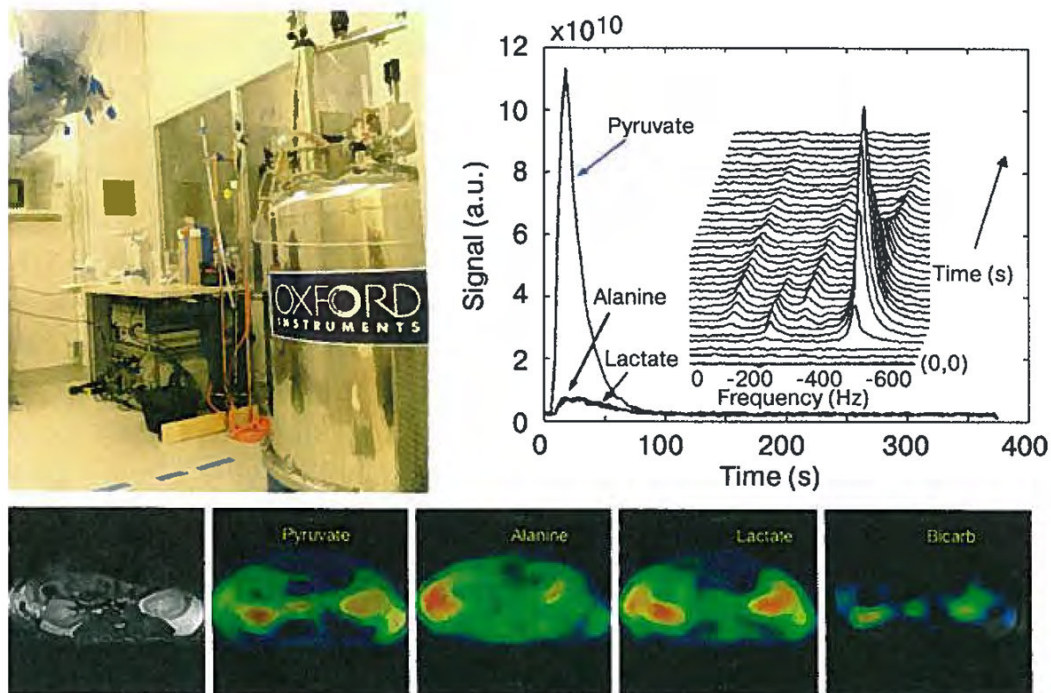


**Fig. 1.**

Prototype DNP polarizer (top left) is in a clean room environment next door to the 3 T MR scanner. Dynamic nonlocalized  $^{13}\text{C}$  MRS are shown (top right) with a 3 s time resolution and demonstrated the uptake of the hyperpolarized  $^{13}\text{C}$ -pyruvate and its metabolic products  $^{13}\text{C}$ -lactate,  $^{13}\text{C}$ -alanine and  $^{13}\text{C}$ -bicarbonate. Metabolite maps from hyperpolarized 2-D  $^{13}\text{C}$  MRSI of a rat (bottom) demonstrate high pyruvate, lactate and bicarbonate in kidney, low pyruvate and lactate in muscle and high alanine in liver. The metabolic images were acquired with a 16 by 16 MRSI sequence in 17 s starting 30 s after injection.

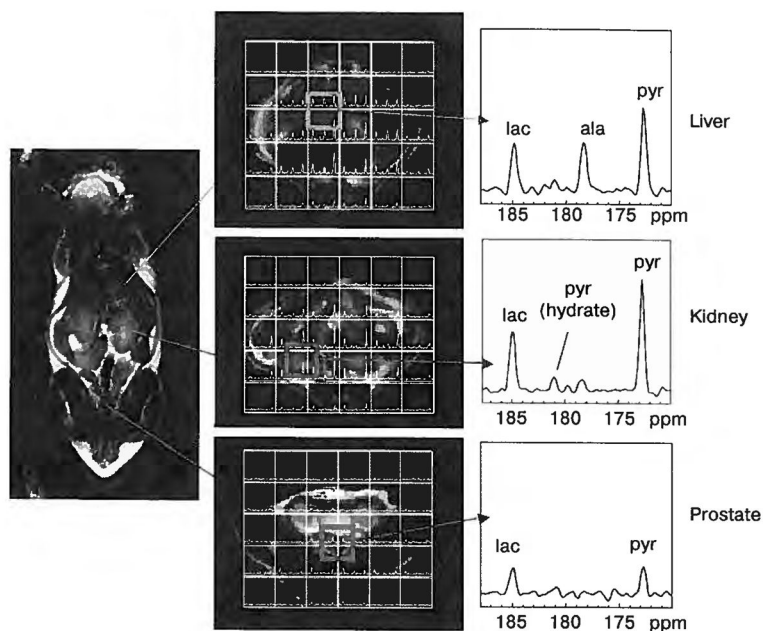


**Fig. 2.** Novel sequence was developed to acquire 3-D spectroscopic data at high spatial resolution in approximately 15 s [29,35]. A coronal  $T_2$ -weighted FSE image from a normal mouse demonstrates the relative location of liver, kidney and prostate. Three axial images through these organs are shown with  $^{13}\text{C}$  spectra obtained from the high-resolution  $^{13}\text{C}$  3-D MRS imaging data ( $0.135\text{ cm}^3$  voxels) overlaid on each image. Individual spectra were voxel-shifted to center on the liver (top), kidney (middle) and prostate (bottom). High levels of pyruvate, alanine, and lactate were observed in liver, while kidney demonstrated high lactate and lower alanine. Low levels of  $^{13}\text{C}$ -pyruvate, as well as  $^{13}\text{C}$ -lactate, were seen in the region of the normal mouse prostate.

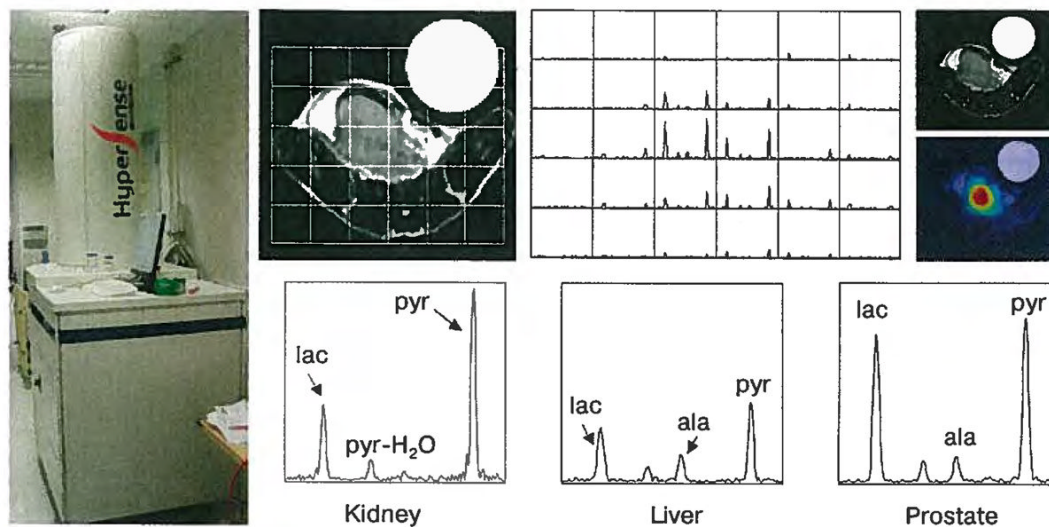


**Fig. 3.**

On the left is a picture of the HyperSense polarizer that is installed between the 7 and 3 T MR scanners at the University of California San Francisco. Selected spectra from the 3-D 8 by 8 by 16 mm  $^{13}\text{C}$  MRS imaging data acquired in 14 s at 3 T demonstrate dramatic increases in  $^{13}\text{C}$ -lactate signals in the transgenic prostate tumor following injection of  $^{13}\text{C}$ -pyruvate that was pre-polarized in the HyperSense system. Lactate S/N ratio was measured to be 59.9 in the kidney and 115.9 in the tumor.

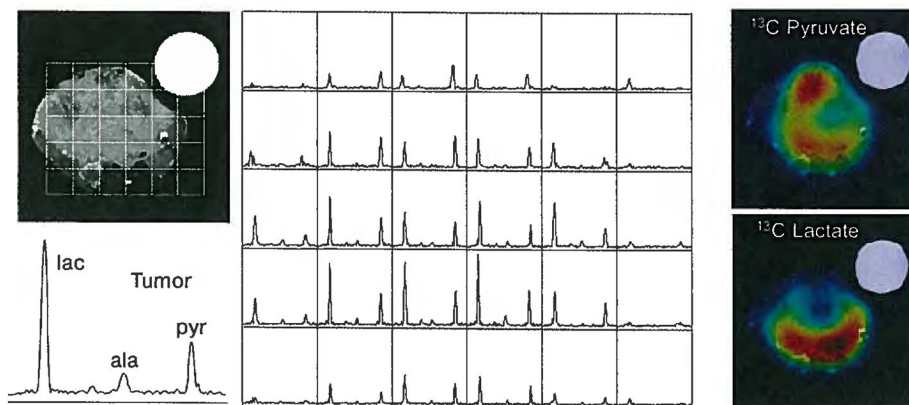


**Fig. 4.** This study of a TRAMP prostate model tumor using the HyperSense system for prepolarization demonstrated not only high  $^{13}\text{C}$ -lactate in the tumor but also differences in metabolite distributions in the tumor. The data were acquired in 14 s and show high uptake of hyperpolarized pyruvate throughout much of the tumor, except for a presumably necrotic region at the center. The lactate image demonstrated a focus of high metabolic activity in the posterior aspect of the tumor, which is indicative of biologically aggressive cancer.

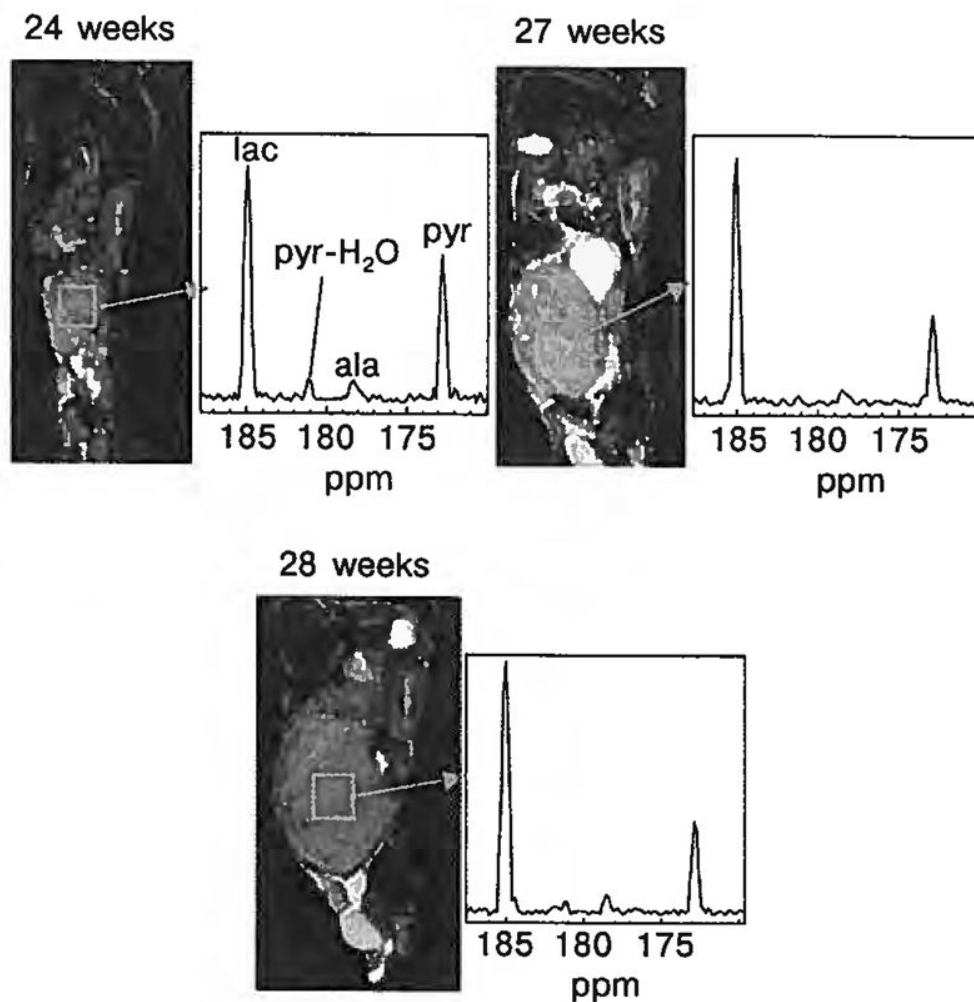


**Fig. 5.** Serial studies of the same TRAMP mouse demonstrate the ability to follow disease progression in this transgenic model of prostate cancer at 24, 27 and 28 weeks. All  $^{13}\text{C}$  MRS imaging data were acquired in 14 s using the 3-D double spin-echo flyback EPSI sequence with a TR of 215 ms, variable spin-echo and a spatial resolution of  $0.135\text{ cm}^3$ . Voxels in the tumor are highlighted with a frame. Note the increase in the size of the tumor over the period of study. The lactate-to-pyruvate ratio in the tumor voxel increases from the 24th to the 27th week time points and is then similar from the 27th to the 28th week interval. This demonstrates the feasibility of this new technique to follow disease progression and to monitor therapeutic response in preclinical cancer models.

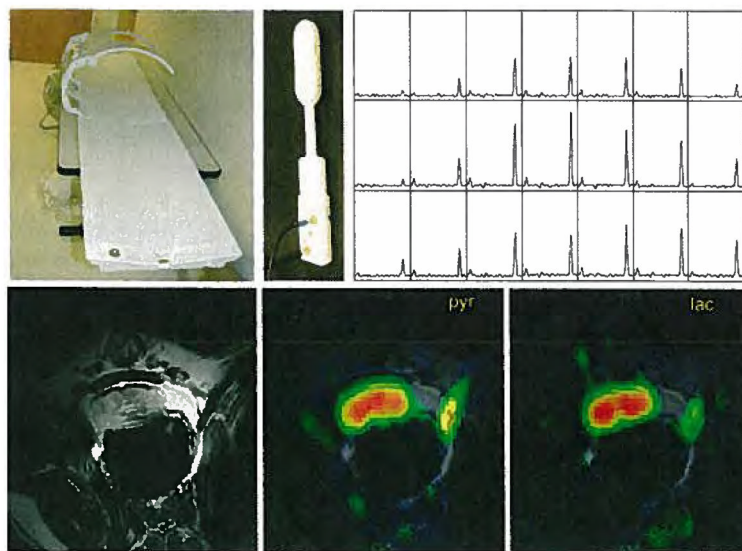


**Fig. 6.** Prototype polarizer has been installed in a clean room adjacent to the 3 T magnet in preparation for studies in prostate cancer patients that will use the coils designs shown on the left. Canine MRSI studies (right) obtained in 15 s at a spatial resolution of  $0.125 \text{ cm}^3$  demonstrated not only feasibility but also high S/N ratio of 200 and higher for  $^{13}\text{C}$ -pyruvate and much lower  $^{13}\text{C}$ -lactate levels than in cancer model systems. These preliminary MR metabolic imaging studies demonstrated sufficient sensitivity to detect metabolism throughout the prostate at a much greater spatial and temporal resolution than previously possible.